WASHINGTON UNIVERSITY IN ST. LOUIS

The report from Washington University for the period follows.

ENGINEERING DEVELOPMENT OF SLURRY BUBBLE COLUMN REACTOR (SBCR) TECHNOLOGY

Sixteenth Quarterly Report
for
January 1 - March 31, 1999

(Budget Year 4: October 1, 1998 – September 30, 1999)

Objectives for the Fourth Budget Year

The main goal of this subcontract from the Department of Energy via Air Products is to study the fluid dynamics of slurry bubble columns and address issues related to scaleup and design. The objectives set for the fourth budget year (October 1, 1998 – September 30, 1999) are listed below.

- Extension of the CARPT/CT database to conditions of industrial interest such as high superficial gas velocity (up to 30-50 cm/s).
- Examination of the improved gas mixing phenomenological model against LaPorte tracer data.
- Critical evaluation of the developed phenomenological models for liquid and gas mixing against the newly obtained data.
- Testing of the 4-points optical probe for bubble sizes and bubble rise velocity measurements.
- Further improvement in Computational Fluid Dynamics (CFD) using CFDLIB and FLUENT through development of improved closure schemes and comparison of two-dimensional (2D) and three-dimensional (3D) model predictions with 2D and 3D data.

In this report, the research progress and achievements accomplished in the sixteenth quarter (January 1 - March 31, 1999) are summarized.

HIGHLIGHTS

Characterization of Gas Phase Mixing Via Gas-Liquid Recirculation Model (GLRM)

- A one-dimensional (1D) model based on the two-fluid approach and the momentum balances for the gas and liquid phase has been developed. The resulting methodology allows the de-coupling of the solution for the liquid/slurry phase momentum balance from the gas phase velocity, which is subsequently calculated based on a suitable drag formulation.

- The computation of the gas phase velocity profile is based on rigorously satisfying the gas phase continuity; and is thereby free from shortcomings resulting from the use of an arbitrary slip velocity correlation for gas velocity computations. Use of such a correlation may violate the integral mass balance for the gas phase.

- The mathematical description for the physically based two bubble-class model for representation of gas phase transport in bubble columns has been developed and is presented in this report.

- The procedure for the estimation of the parameters required in the simulation of the above model equations has been established and is outlined in this report.

- The developed model presents an intermediate step between the empirical axial dispersion models and the full-blown 2D and 3D computational fluid dynamic models for representation of gas flow and transport in bubble columns.

- The model indicates that the time-averaged centerline liquid velocity in the LaPorte reactor during methanol synthesis may be on the order of 1 m/s, while the gas centerline velocity could be as large as 1.5 m/s.

Numerical Simulation of 2D Bubble Column and Quantitative Comparison with PIV Measurements

- The simulations were performed for the 11.2, 15.2, and 10.16 cm columns and for the flow conditions of 1 to 5.49 cm/s superficial gas velocity, 110 and 160 cm static liquid height, 2 and 3 gas injectors, and 7.2 to 15.8 two-phase dispersion height to column diameter aspect ratio.

- Reasonably good agreement between the computed mean quantities--which include liquid velocity, turbulence intensities and Reynolds shear stress—and the PIV data were obtained.

- The characteristics of the large structures, i.e., the wave length and frequency, varied with superficial gas velocity and column dimension. The numerical values were comparable to those obtained by PIV measurements.

1. CHARACTERIZATION OF GAS PHASE MIXING VIA GAS-LIQUID RECIRCULATION MODEL (GLRM)

The interpretation of radioactive tracer runs to characterize mixing of the gas phase in a slurry bubble column during liquid phase methanol synthesis in the LaPorte AFDU reactor was accomplished earlier using the Axial Dispersion Model (ADM) (Degaleesan et al., 1996a). That study clearly showed that the gas tracer data interpretation was more difficult than that for the liquid tracer due to the finite solubility of the tracer (Ar-41). This necessitated modeling of both the gas and liquid phases simultaneously. The gas dispersion coefficients fitted to the tracer responses collected at various elevations did not exhibit a consistent trend, and the values were widely scattered around the mean. This situation was analogous to that observed when the ADM was used to interpret liquid phase tracer runs. Moreover, attempts to extract other parameters from the tracer data, such as volumetric mass transfer coefficients, did not produce consistent results.

In order to remedy this situation, the development of a two-bubble-class, gas-liquid recirculation model, which is based on experimental evidence, has now been completed to overcome some of the inherent inadequacies of the ADM. The details of the initial model formulation and parameter estimation were reported as part of the semiannual report under UCR grant DE FG22 95 PC95212 (Dudukovic' et al., 1996). However, the model development reported there was only preliminary, and no systematic study was undertaken to examine model predictions as a function of the input parameters. In view of the possibilities of using the model as a future scaleup tool, the model has been revisited to incorporate the best available physics to estimate parameters in order to render the model as predictive as possible. We outline here the model structure and some of the developments in estimating model parameters. We also present the detailed model equations, along with the physical basis for this mechanistic model.

1.1 Two-Bubble-Class, Gas-Liquid Recirculation Model

The compartmentalization of the developed mechanistic (phenomenological) model is shown in Figure 1.1 for completeness. The liquid is a batch system, with up-flow (L_1) in the core and down-flow (L_2) near the walls. The extension to situations with net co-current flow of the liquid/slurry is straightforward. The gas phase also has a similar recirculation pattern; however, only small bubbles (SB_2), which do not possess sufficient momentum, get recirculated along with the liquid. The large bubbles (LB), with smaller bubbles (SB_1) trapped in the wakes of these larger bubbles, rise up through the central core due to large buoyancy forces and drag the liquid along with them. The top (disengagement) zone and the bottom (distributor) zone are modeled as CSTRs with uniform (small) bubbles only. The height of these zones is taken to be the same as the column diameter D_c. Changing the height of these zones between 0.5 and 1.0 D_c does not have any noticeable effect on the liquid backmixing [Degaleesan et al., 1996b], as long

as the height of the gas-liquid mixture is much greater than the column diameter (L/D_c of at least 6). The effect of these zones on the gas phase model still needs to be verified.

For the developed part of the flow, which occupies most of the column, five transient convection-diffusion equations with mass transfer between regions as source terms can be written. Additionally, reaction rates appear as source terms in the liquid phase equations if one is simulating a column under reaction conditions. The other source terms come from the large-small bubble interactions in the core of the column.

The developed phenomenological model, schematically shown in Figure 1.1, is based on the currently available physical evidence. The hydrodynamic phenomena observed experimentally through the unique CARPT and CT techniques are represented schematically in Figure 1.2 and form the basis of the mechanistic model described earlier. In a bubble column in the time average sense, a single liquid recirculation loop is established with the liquid rising in the center and flowing downwards by the walls (Degaleesan, 1997). Superimposed on this recirculation is eddy diffusion caused by the bubble wakes. Gas travels in the column via small and large bubbles (Krishna and Ellenberger, 1996), which exchange their contents in the up-flow region. However, only small bubbles are dragged down by the downward flowing liquid. A soluble-gas-tracer experiences mass transfer to the liquid phase, and the mass transfer coefficients for the small and large bubbles are different and have to be evaluated separately.

Figure 1.2 shows the representative liquid and gas velocity profiles. r' and r" are the radial locations at which the time-averaged liquid and gas velocities change sign, respectively, i.e., go to zero. As the gas and liquid velocities reach zero at different radial locations, there is a region between r' and r" where small bubbles are moving up but the liquid is moving down.

1.2 Two-Fluid Model for Gas and Liquid Phase Momentum Exchange

The basis for the derivation of the 1D model for the liquid- and gas-phase-velocity profiles are the two-fluid model equations presented below. These are the result of the ensemble-averaged approach of Drew (1983). The subscript 'c' denotes the continuous liquid/slurry phase, whereas the subscript 'd' denotes the dispersed gas phase. Both phases are considered incompressible.

Equations of Continuity

Liquid/Slurry
$$\frac{\partial \varepsilon_c}{\partial t} + \nabla.\left(\varepsilon_c \mathbf{u}_c\right) = 0 \tag{1.1}$$

Gas
$$\frac{\partial \varepsilon_d}{\partial t} + \nabla.\left(\varepsilon_d \mathbf{u}_d\right) = 0 \tag{1.2}$$

Momentum Equations

Liquid/Slurry:

$$\rho_c \varepsilon_c \left(\frac{\partial \mathbf{u}_c}{\partial t} + \mathbf{u}_c . \nabla \mathbf{u}_c \right) = \rho_c \varepsilon_c \mathbf{g} - \varepsilon_c \nabla p - \left(\mathbf{M}_d + \mathbf{M}_{vm} \right) + \nabla . \left(\varepsilon_c \sigma_c \right) \tag{1.3}$$

Gas:

$$\rho_d \varepsilon_d \left(\frac{\partial \mathbf{u}_d}{\partial t} + \mathbf{u}_d . \nabla \mathbf{u}_d \right) = \rho_d \varepsilon_d \mathbf{g} - \varepsilon_d \nabla p + \left(\mathbf{M}_d + \mathbf{M}_{vm} \right) + \nabla . \left(\varepsilon_d \sigma_d \right) \tag{1.4}$$

In the momentum balance equations, $\mathbf{M}_d$ is the drag force term, while $\mathbf{M}_{vm}$ is the virtual mass term defined below (Drew, 1983).

$$\mathbf{M}_d = \frac{6 \varepsilon_c \varepsilon_d}{\pi d_p^3} \mathbf{F}_d \tag{1.5}$$

with

$$\mathbf{F}_d = \frac{1}{8} \rho_c \pi d_p^2 C_D \left| \mathbf{u}_c - \mathbf{u}_d \right| \left(\mathbf{u}_c - \mathbf{u}_d \right) \tag{1.6}$$

$$C_D = max \left[\frac{24}{Re} \left(1 + 0.15\, Re^{0.687} \right),\ f \frac{8}{3} \frac{Eo}{Eo + 4} \right] \tag{1.7}$$

$$f = \left\{ \frac{1 + 17.67 \varepsilon_c^{9/7}}{18.67 \varepsilon_c^{3/2}} \right\}^2 \tag{1.8}$$

where

$$Eo \equiv Eotvos\ Number \equiv g \rho_c d_p^2 / \gamma$$

and $Re \equiv Bubble\ Reynolds\ Number$

$$\equiv \rho_c d_p \left| \mathbf{u}_c - \mathbf{u}_d \right| / \mu_c$$

$$\mathbf{M}_{vm} = \frac{1}{2} \varepsilon_c \varepsilon_d C_{vm} \left(\frac{D \mathbf{u}_c}{Dt} - \frac{D \mathbf{u}_d}{Dt} \right) \tag{1.9}$$

$$C_{vm} = 1 + 3.32 \varepsilon_d + O(\varepsilon_d^2) \tag{1.10}$$

In the well-developed flow region of the column, the flow in the time-averaged sense is known to be axisymmetric, with only the axial velocities being non-zero. Hence, the time-averaged

liquid flow pattern is represented by a single radial profile of the axial velocity. These assumptions are fair in view of the holdup profile database available at CREL via Computed Tomography (CT); and the liquid velocity profile database via Computer Automated Radioactive Particle Tracking (CARPT).

Under these assumptions, the equations of continuity for both the phases (Equations 1.1 and 1.2) are identically satisfied, and one cannot use the traditional approach of solving the Poisson equation for the pressure correction via these continuity equations (as is done in 2D and 3D CFD codes). In addition, the left-hand side of the momentum equations for both the gas and liquid phase becomes zero, as does the virtual mass term. Finally, due to no flow in the radial and azimuthal directions, the pressure becomes independent of the radial and azimuthal coordinates, and the pressure gradient term in the momentum equations reduces to *dP/dz*.

After retaining the non-zero gradients and velocity components in the momentum equations for the two phases, one obtains the following simplified equations:

Liquid/Slurry
$$0 = -\rho_c \varepsilon_c g - \varepsilon_c \frac{dP}{dz} - M_d + \frac{1}{r}\frac{d}{dr}(r\varepsilon_c \sigma_{c,rz}) \tag{1.11}$$

Gas
$$0 = -\rho_d \varepsilon_d g - \varepsilon_d \frac{dP}{dz} + M_d + \frac{1}{r}\frac{d}{dr}(r\varepsilon_d \sigma_{d,rz}) \tag{1.12}$$

Adding Equations 1.11 and 1.12, one obtains

$$0 = -\left(\overbrace{\rho_d \varepsilon_d}^{negligible} + \rho_c \varepsilon_c \right) g - \frac{dP}{dz} + \frac{1}{r}\frac{d}{dr}(r\tau_{rz}) \tag{1.13}$$

where

$$\tau_{rz} = \varepsilon_c \sigma_{c,rz} + \varepsilon_d \sigma_{d,rz} \tag{1.14}$$

is the effective shear stress of the two-phase mixture. However, since the gas phase viscosity and density are two to three orders of magnitude lower than the liquid/slurry values, the effective shear stress is primarily due to the shear stress of the liquid /slurry phase. Thus, τ_{rz} is the liquid/slurry phase shear stress. A model is needed for this stress, and the simplest closure in terms of turbulent kinematic viscosity is employed in Equation 1.16.

$$\frac{1}{r}\frac{d}{dr}(r\tau_{rz}) = \frac{dP}{dz} + \rho_c (1 - \varepsilon_d) g \tag{1.15}$$

$$\tau_{rz}(r) = -\rho_c(\nu_{c,m} + \nu_{c,t})\frac{du_c}{dr} = -\rho_c\nu_{c,m}\frac{du_c}{dr} - \rho_c l^2\left(\frac{du_c}{dr}\right)^2 \tag{1.16}$$

The turbulent eddy viscosity, $\nu_{c,t}$, is closed by a modified mixing length, $l(\xi)$, as given by Kumar (1994).

$$\nu_{c,t} = l^2\left|\frac{du_c}{dr}\right| \tag{1.17}$$

$$l(\xi) = \frac{a(1-\xi)}{(\xi+b)^c} + d(1-\xi)^e \tag{1.18}$$

The parameters a, b, c, d and e were obtained by Kumar et al. (1994) after extensive data on liquid recirculation velocities from CARPT were considered, as well as results from experiments of other researchers who have made measurements of the liquid recirculation velocity by other experimental means.

At this point, the computation of the radial profile of the axial liquid velocity requires only the gas holdup profile as the input. The circumferentially averaged radial gas holdup profile is frequently represented as follows:

$$\varepsilon_d(\xi) = \overline{\varepsilon_d}\left(\frac{m+2}{m+2-2c}\right)\left(1-c\xi^m\right) \tag{1.19}$$

With the gas holdup profile as input, the liquid velocity profile can be readily computed by a procedure described elsewhere (Kumar, 1994; Kumar et al., 1994).

Once the liquid velocity profile and *dP/dz* are determined from the converged 1D liquid circulation model (Kumar et al., 1994), one returns to the gas phase momentum equation and iterates on the bubble diameter in the drag formulation. In this way, the converged gas phase velocity profile that satisfies the gas phase continuity is obtained.

$$M_d = \varepsilon_d\frac{dP}{dz} + \rho_d\varepsilon_d g \tag{1.20}$$

$$M_d = \frac{6\varepsilon_c\varepsilon_d}{\pi d_p^3}F_d \tag{1.21}$$

$$F_d = -\frac{1}{8}\rho_c\pi d_p^2 C_D\left(u_c - u_d\right)^2 \tag{1.22}$$

Substitution of Equation (1.21) into Equation (1.20) with the help of Equation (1.22) results in the equation from which the gas velocity profile, u_d, is determined. This calculation requires iteration, since the bubble size, d_p, must be guessed and the drag coefficient must be evaluated by Equation 1.7. The guessed bubble size, d_p, is used along with the available gas holdup profile, $\varepsilon_d(\xi)$, from Equation 1.19 and the liquid recirculation velocity calculated from the model, consisting of Equations 1.15-1.19, to obtain the updated u_d. Iteration on the bubble diameter, d_p, continues until the integral gas phase continuity is satisfied.

It should be mentioned that the use of a single bubble size during iteration for the gas velocity profile is to demonstrate the applicability of this novel technique. To be consistent with the overall two-bubble class approach, the existence of two different bubble classes needs to be reflected in the computation of the gas velocity profile as well. A variant to this model is being developed in which the gas phase momentum will be split into separate contributions from the small and large bubbles, along with a momentum interchange term for the two bubble classes. This work is still under development and will be reported upon completion.

1.3 Gas Phase Mixing Model

1.3.1 Assumptions and Model Development

1) The process is semi-batch, but the development can be extended readily for continuous liquid/slurry flow.
2) The interaction between small bubbles moving up (SB_1) and small bubbles moving down (SB_2) is due to radial turbulent diffusion alone.
3) The small bubble coalescence and breakup in the SB_2 region where bubbles are dragged down by the liquid is negligible, as no large bubbles are observed near the wall. To communicate with the large bubbles (LB), the bubbles from SB_2 have to be transported radially via turbulent diffusion to the region SB_1, where they can interact with large bubbles.
4) The axial and radial turbulent diffusivities for the small bubbles and the liquid are assumed to be the same. (If the instantaneous gas velocities are known, one can do away with this assumption, and calculate the gas turbulent diffusivities in the same manner as for the liquid.)
5) The interaction between large bubbles in the upflow region, LB, and small bubbles in the upflow region, SB_1 is due to bubble breakup and coalescence. The mass transfer coefficients (k) for the two bubble classes are calculated based on Higbie's relation, by calculating the contact times based on average bubble diameters and average gas velocities through each bubble phase.
6) Reactions, if any, occur only in the liquid phase. Gas side mass transfer resistance is negligible.

With these assumptions, the 1D mass balances written for all the regions, excluding the CSTRs at the top and bottom, yield five transient, turbulent diffusion-convection partial differential equations (PDEs) with interphase transport, which will be described in the next section. Here we outline the details of the mass balances for one of the compartments of the column into which the fully developed region of the reactor is sectioned, viz., the portion of the column where the small

bubbles move upwards. The source terms are either due to gas-liquid mass transfer or are from exchange due to bubble coalescence and re-dispersion. The exchange between the liquid going up and the liquid going down is expressed in terms of the radial turbulent diffusivity, which is also assumed to characterize the exchange between small bubbles rising and small bubbles travelling downwards.

Figure 1.3 presents the various inputs and outputs to an element of the fully developed region, SB_1, of height dx. The various terms are mathematically represented below (Refer to Figures 1.2 and 1.3).

(Convective + turb. diffusive input)$_x$: $\left(\overline{u}_{g1}\pi\left(r''\right)^2\overline{\varepsilon}_{g1}C_{g1}\right)_x - \overline{D}_{xx_1}\pi\left(r''\right)^2\overline{\varepsilon}_{g1}\left(\frac{\partial C_{g1}}{\partial x}\right)_x$

(Convective + turb. diffusive output)$_{x+dx}$: $\left(\overline{u}_{g1}\pi\left(r''\right)^2\overline{\varepsilon}_{g1}C_{g1}\right)_{x+dx} - \overline{D}_{xx_1}\pi(r'')^2\overline{\varepsilon}_{g1}\left(\frac{\partial C_{g1}}{\partial x}\right)_{x+dx}$

Mass transfer to liquid moving upwards : $k_{su}a_{sulu}(HC_{g1} - C_{l1})(\pi(r'')^2 dx)$

Mass transfer to liquid moving downwards : $k_{su}a_{suld}(HC_{g1} - C_{l2})(\pi(r'')^2 dx)$

Net radial turbulent diffusional exchange between SB1 and SB2 (output):

$$\left[\overline{D}_{rr}\,\varepsilon_g\right]_{r=r''}\left(C_{g1} - C_{g2}\right)dx$$

Net source term for SB1 from bubble breakage and coalescence (input):

$$\left(\frac{\pi}{6}d_S^{*3}\right)\left[-D_{SCL}\right]\left(\pi(r'')^2 dx\right)C_{g1} + \left(\frac{\pi}{6}d_L^{*3}\right)B_{SBL}\left(\pi(r'')^2 dx\right)C_{g3}$$

where d_S^* *and* d_L^* are the Sauter mean diameter of the small and large bubble classes, respectively, and may vary along the height of the reactor.

Therefore, $Accumulation = (Inpout) - (Output) + Generation$ gives,

$$\frac{\partial C_{g1}}{\partial t} = \left\{ \begin{array}{l} \overline{D}_{xx_1} \frac{\partial^2 C_{g1}}{\partial x^2} - \overline{u}_{g1} \frac{\partial C_{g1}}{\partial x} - \frac{\left[\overline{D}_{rr} \varepsilon_g\right]_{r=r''}}{\pi (r'')^2 \overline{\varepsilon}_{g1}} \left(C_{g1} - C_{g2}\right) - \frac{k_{su} a_{suld}}{\overline{\varepsilon}_{g1}} \left(HC_{g1} - C_{l2}\right) \\ - \frac{k_{su} a_{sulu}}{\overline{\varepsilon}_{g1}} \left(HC_{g1} - C_{l1}\right) - D_{SCL} \left(\frac{\pi}{6} d_S^{*3}\right) \left(\frac{C_{g1}}{\overline{\varepsilon}_{g1}}\right) + B_{SBL} \left(\frac{\pi}{6} d_L^{*3}\right) \left(\frac{C_{g3}}{\overline{\varepsilon}_{g1}}\right) \end{array} \right\} \quad (1.23)$$

Similarly, for the other four regions we obtain the following four transient convection-diffusion equations.

For the small bubbles moving downwards (SB_2)

$$\frac{\partial C_{g2}}{\partial t} = \left[\begin{array}{l} \overline{D}_{xx_2} \frac{\partial^2 C_{g2}}{\partial x^2} + \overline{u}_{g2} \frac{\partial C_{g2}}{\partial x} + \frac{1}{\pi\left(R^2 - (r'')^2\right)} \frac{\left[\overline{D}_{rr} \varepsilon_g\right]_{r=r''}}{\overline{\varepsilon}_{g2}} \left(C_{g1} - C_{g2}\right) \\ - \left[\frac{k_{sd} a_{sdld}}{\overline{\varepsilon}_{g2}}\right] \left((HC_{g2} - C_{l2})\right) \end{array} \right] \quad (1.24)$$

For the large bubbles moving upwards (in plug flow)(SB_3)

$$\frac{\partial C_{g3}}{\partial t} = \left[\begin{array}{l} - \overline{u}_{g3} \frac{\partial C_{g3}}{\partial x} - \left[\frac{k_{Lu} a_{Lu}}{\overline{\varepsilon}_{g3}}\right] \left((HC_{g3} - C_{l1})\right) \\ + \left(\frac{\pi}{6} d_S^{*3} B_{LCS} C_{g1} - \frac{\pi}{6} d_L^{*3} D_{LBS} C_{g3}\right) \frac{1}{\overline{\varepsilon}_{g3}} \end{array} \right] \quad (1.25)$$

For the liquid moving upwards (L_1)

$$\frac{\partial C_{l1}}{\partial t} = \left[\begin{array}{l} \overline{D}_{xx_1} \frac{\partial^2 C_{l1}}{\partial x^2} - \overline{u}_{l1} \frac{\partial C_{l1}}{\partial x} - \frac{1}{\pi (r')^2} \frac{\left[\overline{D}_{rr} \varepsilon_l\right]_{r=r'}}{\overline{\varepsilon}_{l1}} \left(C_{l1} - C_{l2}\right) - Rx_{l1} \\ + \left[\left(\frac{r''}{r'}\right)^2 \frac{1}{\overline{\varepsilon}_{l1}}\right] \left(k_{Lu} a_{Lu} (HC_{g3} - C_{l1}) + k_{su} a_{sulu} (HC_{g1} - C_{l1}) \right) \end{array} \right] \quad (1.26)$$

For the liquid moving downwards (L_2)

$$\frac{\partial C_{l2}}{\partial t} = \left[\begin{array}{l} \overline{D}_{xx_2}\frac{\partial^2 C_{l2}}{\partial x^2} + \overline{u}_{l2}\frac{\partial C_{l2}}{\partial x} + \frac{1}{\pi\left(R^2-(r')^2\right)}\frac{\left[\overline{D}_{rr}\,\varepsilon_l\right]_{r=r'}}{\overline{\varepsilon}_{l2}}\left(C_{l1}-C_{l2}\right) - Rx_{l2} \\ +\left[\frac{k_{sd}}{\overline{\varepsilon}_{l2}\left(R^2-(r')^2\right)}\right]\left((r'')^2 a_{Stulu}(HC_{g1}-C_{l2}) + \left(R^2-(r'')^2\right)a_{Sdld}(HC_{g2}-C_{l2})\right) \end{array}\right] \quad (1.27)$$

It must be noted that these equations are valid only in the regions excluding the two CSTRs. The CSTR at the distributor has a volume V_a and that at the top, a volume equal to V_b. Each CSTR can be split into two volumes, one occupied by the gas and other by the liquid. Thus, applying the mass balance to these volumes, we obtain the following:

Distributor zone

For the liquid phase:

$$\frac{dC_{la}}{dt} = \frac{\overline{\varepsilon}_{l2}}{\overline{\varepsilon}_l}\frac{\left(R^2-(r')^2\right)}{R^2}\frac{\overline{u}_{l2}}{D_C}C_{l2,0} - \frac{\overline{\varepsilon}_{l1}}{\overline{\varepsilon}_l}\frac{r'^2}{R^2}\frac{\overline{u}_{l1}}{D_C}C_{la} + \frac{k_{CSTR}a_{CSTR}}{\overline{\varepsilon}_l}\left(HC_{ga}-C_{la}\right) - Rx_{la} \quad (1.28)$$

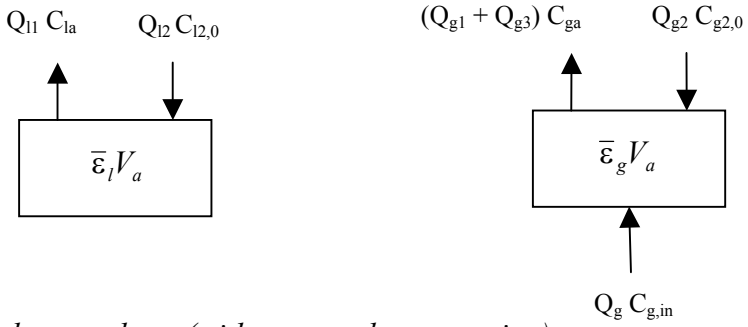

For the gas phase (with no gas phase reaction):

$$\frac{dC_{ga}}{dt} = \left[\begin{array}{l} \frac{\overline{\varepsilon}_{g2}}{\overline{\varepsilon}_g}\frac{\left(R^2-(r'')^2\right)}{R^2}\frac{\overline{u}_{g2}}{D_C}C_{g2,0} - \frac{\left(\overline{\varepsilon}_{g1}\overline{u}_{g1}+\overline{\varepsilon}_{g3}\overline{u}_{g3}\right)}{\overline{\varepsilon}_g D_C}\frac{r''^2}{R^2}C_{ga} \\ +\frac{U_G}{\overline{\varepsilon}_g D_C}C_{g,in} - \frac{k_{CSTR}a_{CSTR}}{\overline{\varepsilon}_g}\left(HC_{ga}-C_{la}\right) \end{array}\right] \quad (1.29)$$

Disengagement zone

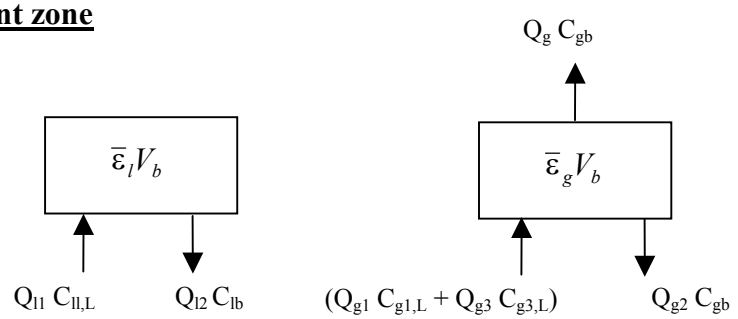

For the liquid phase:

$$\frac{dC_{lb}}{dt} = \frac{\bar{\varepsilon}_{l1}}{\bar{\varepsilon}_l}\frac{r'^2}{R^2}\frac{\bar{u}_{l1}}{D_C}C_{l1,L} - \frac{\bar{\varepsilon}_{l2}}{\bar{\varepsilon}_l}\frac{\left(R^2-(r')^2\right)}{R^2}\frac{\bar{u}_{l2}}{D_C}C_{lb} + \frac{k_{CSTR}a_{CSTR}}{\bar{\varepsilon}_l}\left(HC_{gb}-C_{lb}\right) - Rx_{lb} \qquad (1.30)$$

For the gas phase (with no gas phase reaction):

$$\frac{dC_{gb}}{dt} = \left[\begin{array}{l} \dfrac{\left(\bar{\varepsilon}_{g1}\bar{u}_{g1}C_{g1,L} + \bar{\varepsilon}_{g3}\bar{u}_{g3}C_{g3,L}\right)}{\bar{\varepsilon}_g D_C}\dfrac{r''^2}{R^2} - \dfrac{\bar{\varepsilon}_{g2}}{\bar{\varepsilon}_g}\dfrac{\left(R^2-(r'')^2\right)}{R^2}\dfrac{\bar{u}_{g2}}{D_C}C_{gb} \\ -\dfrac{U_G}{\bar{\varepsilon}_g D_C}C_{gb} - \dfrac{k_{CSTR}a_{CSTR}}{\bar{\varepsilon}_g}\left(HC_{gb}-C_{lb}\right) \end{array}\right] \qquad (1.31)$$

The equations above are ordinary differential equations (ODEs) and require only the initial conditions. For the fully developed sections, initial as well as boundary conditions are required. These are discussed next.

Initial Conditions

A step input of gas tracer at the inlet (bottom) of the column is assumed, with no tracer originally present in the column.

$t = 0; \quad C_{g,in} = H(t)$ (1.32)

$$C_{la} = C_{lb} = C_{ga} = C_{gb} = C_{l1} = C_{l2} = C_{g1} = C_{g2} = C_{g3} = 0 \qquad (1.33)$$

Alternatively, an experimental impulse input can be simulated with a Gaussian function with a tail. Details on this alternative can be found in Degaleesan (1997).

Boundary conditions for the fully developed region

Danckwerts boundary conditions are used at inlet and exit, guaranteeing preservation of mass balance for each phase.

Upflow section of the liquid

At the bottom of the fully developed flow zone, i.e., at the boundary with the CSTR representing the distributor zone:

$$x=0; \qquad \overline{u}_{l1} C_{la} = \overline{u}_{l1} C_{l1}|_{x=0} - D_{xx_1} \frac{\partial C_{l1}}{\partial x}|_{x=0} \tag{1.34}$$

At the top of the fully developed flow zone, i.e., at the boundary with the CSTR representing the disengagement zone:

$$x=L; \qquad \frac{\partial C_{l1}}{\partial x}|_{x=L} = 0 \tag{1.35}$$

Downflow section of the liquid

At the top of the fully developed flow zone, i.e., at the boundary with the CSTR representing the disengagement zone:

$$x=L; \qquad \overline{u}_{l2} C_{lb} = \overline{u}_{l2} C_{l2}|_{x=L} + D_{xx_2} \frac{\partial C_{l2}}{\partial x}|_{x=L} \tag{1.36}$$

At the bottom of the fully developed flow zone, i.e., at the boundary with the CSTR representing the distributor zone:

$$x=0; \qquad \frac{\partial C_{l2}}{\partial x}|_{x=0} = 0 \tag{1.37}$$

Upflow of small bubbles

At the bottom of the fully developed flow zone, i.e., at the boundary with the CSTR representing the distributor zone:

$$x=0; \qquad \overline{u}_{g1} C_{ga} = \overline{u}_{g1} C_{g1}|_{x=0} - D_{xx_1} \frac{\partial C_{g1}}{\partial x}|_{x=0} \tag{1.38}$$

At the top of the fully developed flow zone, i.e., at the boundary with the CSTR representing the disengagement zone:

x=L; $$\frac{\partial C_{g1}}{\partial x}|_{x=L} = 0 \qquad (1.39)$$

Downflow of small bubbles

At the top of the fully developed flow zone, i.e., at the boundary with the CSTR representing the disengagement zone:

x=L; $$\overline{u}_{g2} C_{gb} = \overline{u}_{g2} C_{g2}|_{x=L} + D_{xx_2} \frac{\partial C_{g2}}{\partial x}|_{x=L} \qquad (1.40)$$

At the bottom of the fully developed flow zone, i.e., at the boundary with the CSTR representing the distributor zone:

x=0; $$\frac{\partial C_{g2}}{\partial x}|_{x=0} = 0 \qquad (1.41)$$

Upflow of large bubbles

At the bottom of the fully developed flow zone, i.e., at the boundary with the CSTR representing the distributor zone:

x=0; $$C_{g3}|_{x=0} = C_{ga} \qquad (1.42)$$

1.3.2 Parameter Estimation

The estimation of the various model parameters is outlined in this section. Some of these parameters are estimated based on literature correlations; others are calculated by averaging the velocity and holdup profiles obtained by CARPT/CT.

I. Parameters Estimated from Correlations

Holdup of small bubbles

$$\varepsilon_{small} = 0.5 \exp\left(-193 \rho_g^{-0.61} \eta_l^{0.5} \sigma^{0.11}\right) \qquad \text{(Wilkinson et al., 1992)} \qquad (1.43)$$

Sauter mean diameter of small bubbles

$$d_S^* = 3 g^{-0.44} \sigma^{0.34} \eta_l^{0.22} \rho_l^{-0.45} \rho_g^{-0.11} U_G^{-0.02} \qquad \text{(Wilkinson et al., 1994)} \qquad (1.44)$$

Superficial velocity of small bubbles

$$U_{df} = 2.25\varepsilon_{small}\frac{\sigma}{\eta_l}\left(\frac{\sigma^3\rho_l}{g\eta_l^4}\right)^{-0.273}\left(\frac{\rho_l}{\rho_g}\right)^{0.03} \qquad \text{(Wilkinson et al., 1992)} \qquad (1.45)$$

Sauter mean diameter of large bubbles

$$d_L^* = \left(U_G - U_{df}\right)^{2/5}(h^* + h_0)^{4/5}g^{-1/5} \qquad \text{(de Swart, 1996)} \qquad (1.46)$$

Bubble size stabilization height above the gas distributor

$$h^* = 0.73\left(U_G - U_{df}\right) \qquad \text{(de Swart, 1996)} \qquad (1.47)$$

The gas holdup is assumed to vary radially as (Kumar, 1994)

$$\varepsilon_g(\zeta) = \bar{\varepsilon}_g\left(\frac{m+2}{m}\right)\left(1 - c\zeta^m\right) \qquad (1.48)$$

where ζ is the dimensionless radius. With the holdup profile parameter ($\overline{\varepsilon_g}$, m and c) being either determined experimentally or estimated by the procedure outlined by Degaleesan (1997), the gas and liquid velocity profiles are computed by the methodology outlined in the previous monthly report.

II. Computed Parameters

The fraction of the inlet flow rate of the gas, which travels up the column as large bubbles, is then computed as

$$\alpha = \frac{U_G - U_{df}}{U_G} \qquad (1.49)$$

With the knowledge of the radial profile of gas holdup and gas and liquid velocity profiles, the following average quantities can be computed:

Average holdup of the liquid ascending

$$\bar{\varepsilon}_{l1} = \frac{2}{r'^2}\int_0^{r'}(1-\varepsilon_g)rdr \tag{1.50}$$

Average holdup of the liquid descending

$$\bar{\varepsilon}_{l2} = \frac{2}{\left(R^2-(r')^2\right)}\int_{r'}^{R}(1-\varepsilon_g)rdr \tag{1.51}$$

Average holdup of the gas ascending

$$\bar{\varepsilon}_{g1} + \bar{\varepsilon}_{g3} = \frac{2}{r''^2}\int_0^{r''}\varepsilon_g rdr \tag{1.52}$$

This equation cannot give us the two holdups separately and, therefore we need another independent equation. In the absence of independent measurements, the holdup of either large or of small bubbles can be calculated using a literature correlation. For this work, equation 1.43 is used to calculate the holdup of small bubbles.

Average holdup of the small bubbles descending

$$\bar{\varepsilon}_{g2} = \frac{2}{\left(R^2-(r'')^2\right)}\int_{r''}^{R}\varepsilon_g rdr \tag{1.53}$$

Average holdup of the small bubbles ascending with liquid descending

$$\bar{\varepsilon}'_{g1} = \frac{2}{\left(r''\right)^2}\int_{r'}^{r''}\varepsilon_g r\,dr \tag{1.54}$$

Average velocity of the liquid ascending

$$\bar{u}_{l1} = \frac{2\int_0^{r'}(1-\varepsilon_g)\,u_l\,r\,dr}{r'^2\,\bar{\varepsilon}_{l1}} \tag{1.55}$$

Average velocity of the liquid descending

$$\overline{u}_{l2} = \frac{2\int_{r'}^{R}(1-\varepsilon_g)\,u_l\,r\,dr}{\left(R^2-(r')^2\right)\overline{\varepsilon}_{l2}} \tag{1.56}$$

Average velocity of the small bubbles ascending

$$\overline{u}_{g1} = \frac{(1-\alpha)R^2U_G + 2\int_{r''}^{R}\left|u_g\right|\varepsilon_g\,r dr}{r''^2\,\overline{\varepsilon}_{g1}} \tag{1.57}$$

Average velocity of the large bubbles ascending

$$\overline{u}_{g3} = \frac{\alpha R^2 U_G}{r''^2\,\overline{\varepsilon}_{g3}} \tag{1.58}$$

Average velocity of the small bubbles descending

$$\overline{u}_{g2} = \frac{2\int_{r''}^{R}\left|u_g\right|\varepsilon_g\,r dr}{\left(R^2-(r'')^2\right)\overline{\varepsilon}_{g2}} \tag{1.59}$$

Interfacial area for mass transfer from small bubbles moving up to liquid moving up

$$a_{sulu} = \frac{6\left(\overline{\varepsilon}_{g1}-\overline{\varepsilon}'_{g1}\right)}{d_S^*} \tag{1.60}$$

Interfacial area for mass transfer from small bubbles moving up to liquid moving down

$$a_{suld} = \frac{6\left(\overline{\varepsilon}'_{g1}\right)}{d_S^*} \tag{1.61}$$

Interfacial area for mass transfer from small bubbles moving down to liquid moving down

$$a_{sdld} = \frac{6\left(\overline{\varepsilon}_{g2}\right)}{d_S^*} \tag{1.62}$$

Interfacial area for mass transfer from large bubbles to liquid moving up

$$a_{Lu} = \frac{6\left(\overline{\varepsilon}_{g3}\right)}{d_L^*} \tag{1.63}$$

Interfacial area for mass transfer in CSTRs

$$a_{CSTR} = \frac{6\left(\overline{\varepsilon}_g\right)}{d_S^*} \tag{1.64}$$

Mass transfer coefficient from small bubbles to liquid moving up

$$k_{su} = \frac{2}{\sqrt{\pi}}\sqrt{\frac{D_{L,m}\,\overline{u}_{g1}}{d_S^*}} \tag{1.65}$$

Mass transfer coefficient from small bubbles to liquid moving down

$$k_{sd} = \frac{2}{\sqrt{\pi}}\sqrt{\frac{D_{L,m}\,\overline{u}_{g2}}{d_S^*}} \tag{1.66}$$

Mass transfer coefficient from large bubbles to liquid moving up

$$k_{Lu} = \frac{2}{\sqrt{\pi}}\sqrt{\frac{D_{L,m}\,\overline{u}_{g3}}{d_L^*}} \tag{1.67}$$

Mass transfer coefficient in CSTRs

$$k_{CSTR} = \frac{2}{\sqrt{\pi}}\sqrt{\frac{D_{L,m}\,U_G}{\overline{\varepsilon}_g\, d_S^*}} \tag{1.68}$$

1.4 Remarks

The protocol outlined above has been established to evaluate all parameters required as input in the solution of the two-bubble class model equations, for simulation of tracer and/or reactor performance (reaction is considered only in the liquid phase). As can be seen from these equations, the number of required hydrodynamic inputs increases dramatically the physics of the flow in such systems is explored in detail. This emphasizes the fact that the coupling between mass and momentum transfer in such systems is very complicated and is precisely the reason for the inadequacy of the Axial Dispersion Model (ADM) for predictive purposes. It is therefore necessary to try to incorporate as much physics as is possible into the mathematical models to represent the phenomena in slurry bubble columns.

A critical evaluation of some of the parameters outlined above for the case of a typical operating condition at the LaPorte AFDU is in progress. Some alternative forms and procedures for

improved parameter estimation based on the latest reports in the literature are being explored. This includes an analysis of the consistency of the evaluated parameters and the form of the convection diffusion PDEs.

1.5 Results and Discussion

In this report, simulation results for the estimated liquid and gas velocity profiles are presented for the case of the LaPorte reactor operated under high-pressure conditions. The operating conditions for the various runs are listed in Table 1.1. The column diameter for this case was 0.46 m. At the operating conditions for the runs, the effective slurry viscosity was 0.99 cP, and the effective slurry density was 995 kg/m^3.

Table 1.1. Operating Conditions during Tracer Runs

Run	Op. Pressure (MPa)	Op. Temperature (^{0}C)	$Ug_{sup,avg}$ (cm/s)	$\overline{\varepsilon_d}$
14.6	5.2	250	22.86	0.39
14.7	5.2	250	12.66	0.33
14.8	3.6	250	32.81	0.38

For these experiments, Differential Pressure (DP) and Nuclear Density Gauge (NDG) measurements were conducted at each operating condition. The DP measurements provide the average gas holdup ($\overline{\varepsilon_d}$), whereas from NDG measurements the chordal average holdup along the diameter is obtained. The constant c in the gas holdup profile of Equation (1.19) is obtained (assuming a value of 2 for the exponent m as reported in the previous study by Degaleesan et al., 1996). This yields the parameters in the gas holdup profile as listed in Table 1.2.

Table 1.2. Parameters in the Gas Holdup Profile

Run	$\overline{\varepsilon_d}$	M	C
14.6	0.39	2	0.844
14.7	0.33	2	0.891
14.8	0.38	2	0.943

Figures 1.4 and 1.5 show the liquid and gas velocity profiles, respectively, computed from the one-dimensional momentum balance equations for the liquid and gas phases as illustrated above. The figures show that the 1D model has been able to effectively capture the recirculation of both the gas and liquid phases. The model predicts a centerline slip velocity of about 50 cm/s, which appears to be high. Such a high slip velocity could be due to several causes:

- Only two independent measurements are available to calculate the three parameters in the gas holdup profile (Equation 1.19). Thus, the profile cannot be determined uniquely, and one of the parameters has to be fixed to evaluate the other two. For the present case the parameter chosen was the exponent m, whose value was fixed at 2 as is customarily reported in the literature for columns operated under churn-turbulent flow conditions at atmospheric pressures. The assumption of m being 2 might not be reasonable based on our experience with a laboratory-scale, high-pressure bubble column, in which values of m in the range of 2.9-3.5 have been normally observed. Since the AFDU is operated at pressures exceeding the highest operating pressure of our laboratory unit, the use of m = 2 becomes questionable. The exponent m determines the gradient of the gas holdup profile, which is the main driving force for liquid recirculation, and thus, influences the calculation of the pressure drop as well. Therefore, the calculation of the slip velocity may be indirectly influenced by an inaccurate choice of the gas holdup profile. However, the purpose of these results is to demonstrate what the model can do, provided a correct gas holdup profile is available.

- A single bubble size has been used to represent the gas phase in the entire cross section. However, this is not the case, as evidenced by experimental observations. As mentioned earlier, a modified model is being derived to account for the presence of two bubble classes.

Additionally, further investigations are under way to evaluate the possible importance of other terms in the interaction forces between the phases. However, at present, it is believed that drag is the main contribution to the interphase interaction.

The liquid and gas velocity profiles, along with other input parameters, provide the information necessary for the simulation of tracer responses. The complete mathematical representation of the two-bubble class gas-liquid recirculation model, as well as the procedure for parameter estimation, will be provided in subsequent monthly reports.

Nomenclature

a	interfacial area, cm^{-1}
B	number of bubbles formed per unit volume per unit time, # cm^{-3} s^{-1}
C	concentration, moles/cm^3
c	parameter in the holdup profile to allow non-zero holdup at the wall
D	number of bubbles disappearing per unit volume per unit time, # cm^{-3} s^{-1}
D_C	column diameter, cm
$D_{L,m}$	molecular diffusivity, cm^2/s
$\overline{D}_{rr}$	radial turbulent diffusivity, cm^2/s
$\overline{D}_{xx_1}$	axial turbulent diffusivity of small bubbles and liquid ascending, cm^2/s
$\overline{D}_{xx_2}$	axial turbulent diffusivity of small bubbles and liquid descending, cm^2/s

d^*	mean bubble diameter, cm
g	acceleration due to gravity, cm^2/s
H	Henry's constant
h^*	height above the gas distributor, m
h_0	parameter determining the initial bubble size, $h_0 = 0.03$ m
k	mass transfer coefficient, cm/s
L	dispersion height between the two CSTRs, cm
m	power law exponent in the radial gas holdup profile
P	operating pressure, $dyne/cm^2$
Q	gas flow rate, cm^3/s
R	column radius, cm
Rx	reaction rate (in the liquid phase), moles cm^{-3} s^{-1}
r	radial position in the column, cm
r'	radius at which the liquid velocity profile inverts
r''	radius at which the gas velocity profile inverts
T	operating temperature, K
t	time, s
t_c	contact time of the liquid eddies with the bubbles, s
U_G	gas superficial velocity, cm/s
U_L	liquid superficial velocity, cm/s
U_{df}	gas superficial velocity through small bubbles, cm/s
u	velocity, cm/s
$\bar{u}$	radially averaged mean velocity, cm/s
u_l	local liquid velocity in the liquid upflow region, cm/s
V_a	volume in CSTR A, cm^3
V_b	volume in CSTR B, cm^3
V_{bL}	rise velocity of large bubbles in quiescent liquid, cm/s
V_{bS}	rise velocity of small bubbles in quiescent liquid, cm/s
x	axial position in the column, cm

Greek Symbols

α	fraction of the inlet gas flow rate going through large bubbles
ε	phase holdup
$\bar{\varepsilon}$	radially averaged phase holdup
$\bar{\varepsilon}'_{g1}$	mean holdup of small bubbles ascending with liquid descending
γ	surface tension of the liquid, Pa-m
η_l	slurry viscosity, cP
ρ	density, kg/m^3
σ	stress tensor
υ_g	kinematic viscosity of the gas, cm^2/s
υ_m	kinematic viscosity of the liquid, cm^2/s
υ_t	turbulent viscosity of the liquid, cm^2/s
τ	effective shear stress

ζ	dimensionless radius
ζ'	dimensionless radius at which the liquid velocity profile inverts
ζ''	dimensionless radius at which the gas velocity profile inverts

Subscripts

b	bubble
CSTR	CSTRs A and B
g	gas
g1	small bubbles ascending
g2	small bubbles descending
g3	large bubbles ascending
L	large bubbles
LBS	large bubbles breaking into small bubbles
LCS	large bubble from coalescence of small bubbles
Lu	large bubbles ascending with liquid descending
l	liquid
la	liquid phase in the distributor zone, CSTR A
lb	liquid phase in the disengagement zone, CSTR B
l1	liquid ascending
l2	liquid descending
S	small bubbles
LBL	large bubbles due to breakage of/into large bubbles
LBS	large bubbles due to breakage into small bubbles
LCL	large bubbles due to coalescence of/into large bubbles
LCS	large bubbles due to coalescence of small bubbles
SBL	small bubbles from breakage of large bubbles
SBS	small bubbles due to breakage of/into small bubbles
SCS	small bubbles due to coalescence of/into small bubbles
SCL	small bubbles due to coalescence into large bubbles
sd	small bubbles descending
sdld	small bubbles descending with liquid descending as well
su	small bubbles ascending
suld	small bubbles ascending with liquid descending
sulu	small bubbles ascending with liquid ascending as well

References

Degaleesan, S., "Fluid dynamic measurements and modeling of liquid mixing in bubble columns," *D.Sc. Thesis*, Washington University (1997).

Degaleesan, S., M. P. Dudukovic', B. L. Bhatt, and B. A. Toseland, "Slurry bubble column hydrodynamics: tracer studies of the LaPorte AFDU reactor during methanol synthesis," *Fourth Quarterly Report for Contract DOE-FC 2295 PC 95051* (1996a).

Degaleesan, S., S. Roy, S. B. Kumar, and M. P. Dudukovic', "Liquid backmixing based on convection and turbulent dispersion in bubble columns," *Chem. Engng Sci.*, 51, 1967 (1996b).

Drew, D. A., "Mathematical modeling of two-phase flow," *Ann. Rev. Fluid Mech.*, 15, 261 (1983).

Dudukovic', M. P., L. S. Fan, Y. B. Yang, S. D. Degaleesan, and P. Gupta, "Novel techniques for slurry bubble column hydrodynamics*," Second Semiannual Report for Contract DOE-FG 2295 PC 95212* (1996).

Krishna, R. and J. Ellenberger, "Gas holdup in bubble column reactors operating in the churn-turbulent flow regime," *AIChE J.*, 42(9), 2627 (1996).

Kumar, S. B., N. Devanathan, D. Moslemian, and M. P. Dudukovic', "Effect of scale on liquid recirculation in bubble columns," *Chem. Engng Sci.*, 49(24B), 5637 (1994).

Kumar, S. B., "Computed tomographic measurements of void fraction and modeling of the flow in bubble columns," *Ph.D. Thesis*, Florida Atlantic University (1994).

de Swart, J. W. A., "Scaleup of a Fischer-Tropsch slurry reactor," Ph. D. Thesis, University of Groningen, The Netherlands (1996).

Wilkinson, P. M., H. Haringa, and L. L. van Dierendonck, "Design parameters estimation for scaleup of high pressure bubble columns," *Chem. Eng. Sci.*, 49, 1417 (1994).

Wilkinson, P. M., A. P. Spek, and L. L. van Dierendonck, "Mass transfer and bubble size in a column under pressure," *AIChE J.*, 38, 544 (1992).

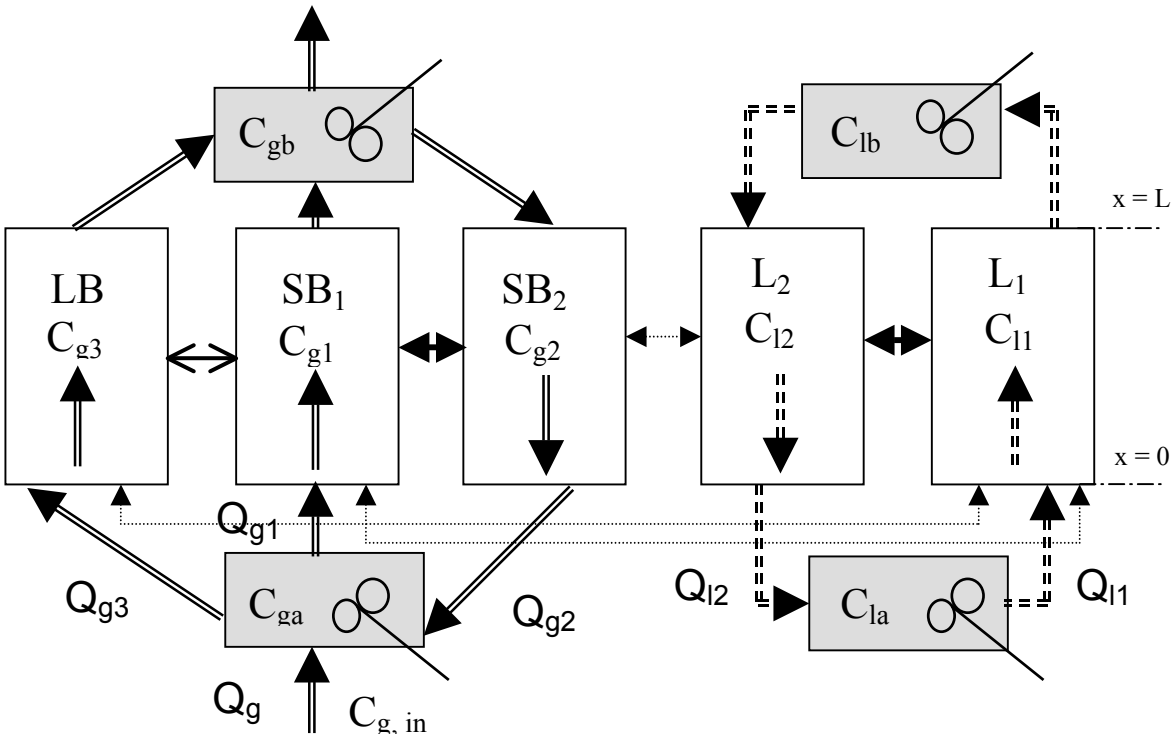

Figure 1.1 Schematic Representation of the Compartmentalization of the Reactor

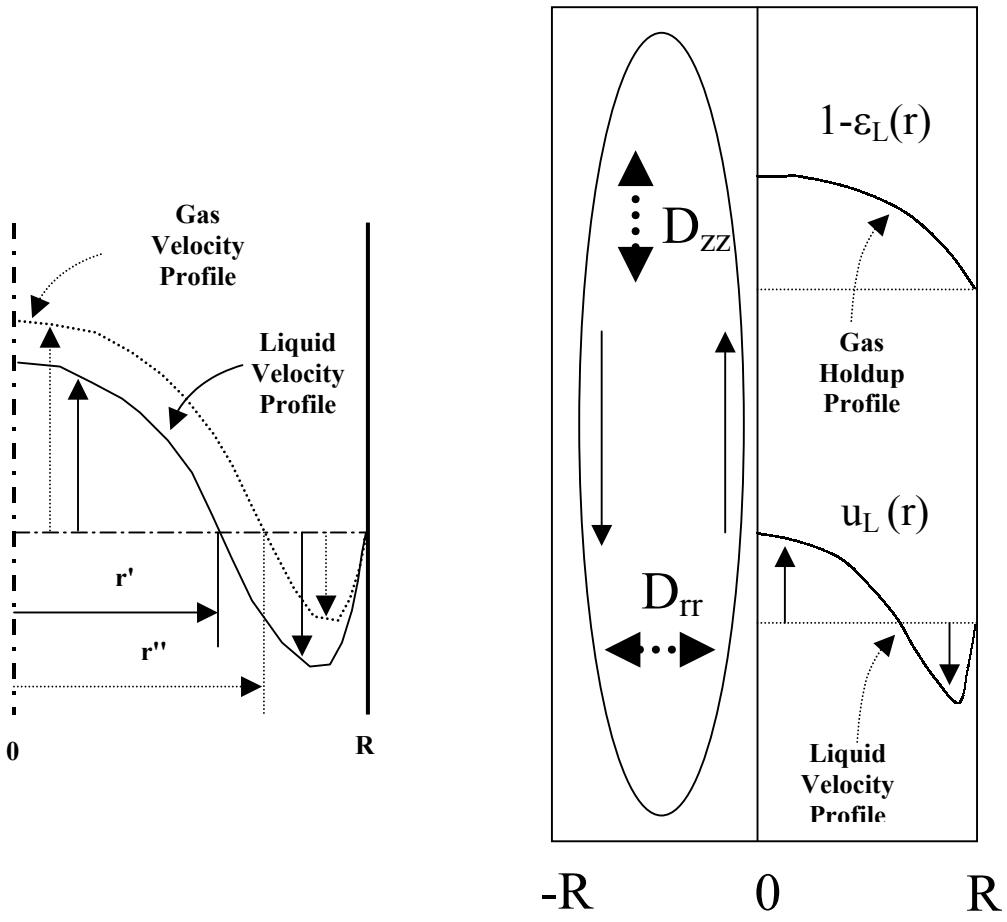

Figure 1.2 Schematic Representation of the Experimentally Observed Phenomena in Bubble Columns

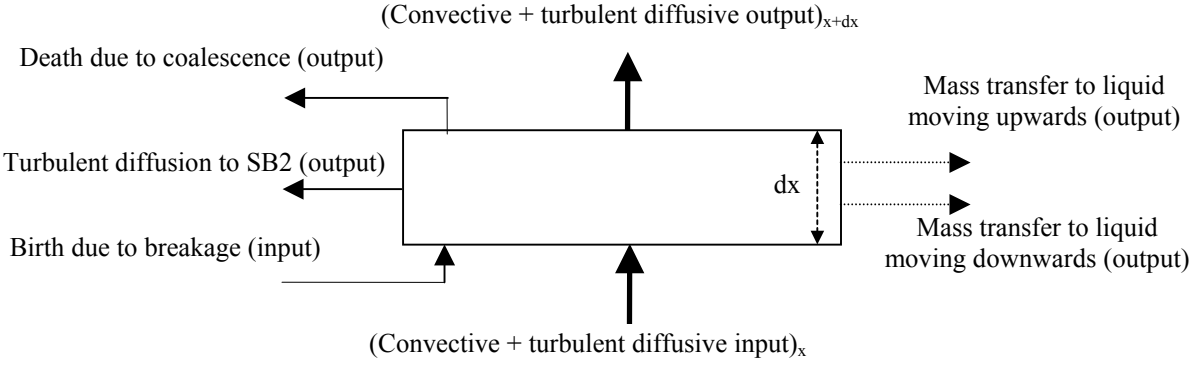

Figure 1.3 Details of 1D Mass Balance for the Small Bubbles Ascending

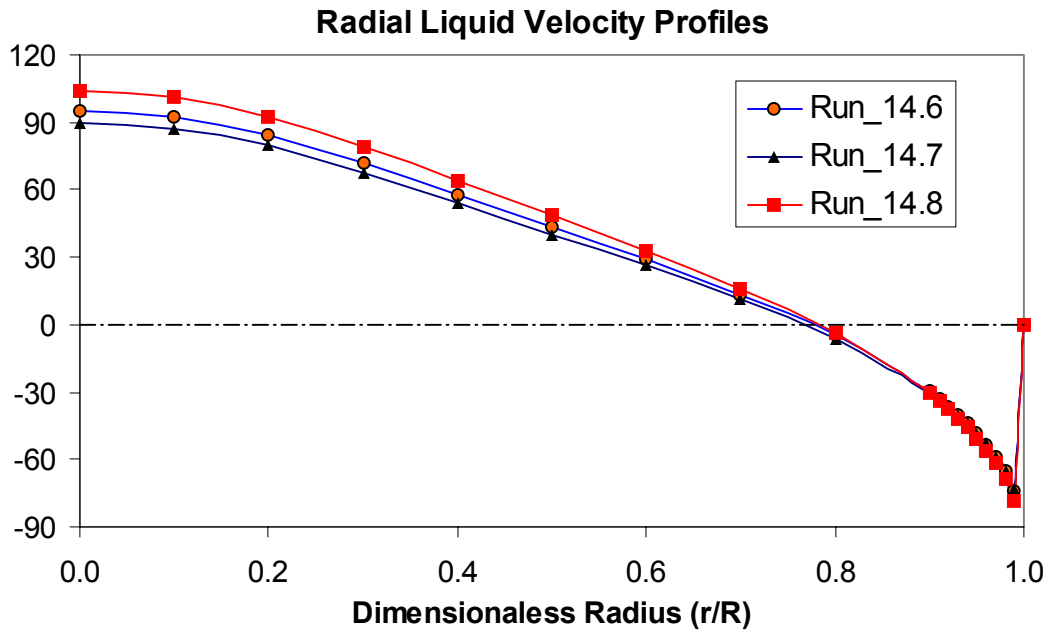

Figure 1.4 Computed 1D Liquid Velocity Profiles for the Three Operating Conditions

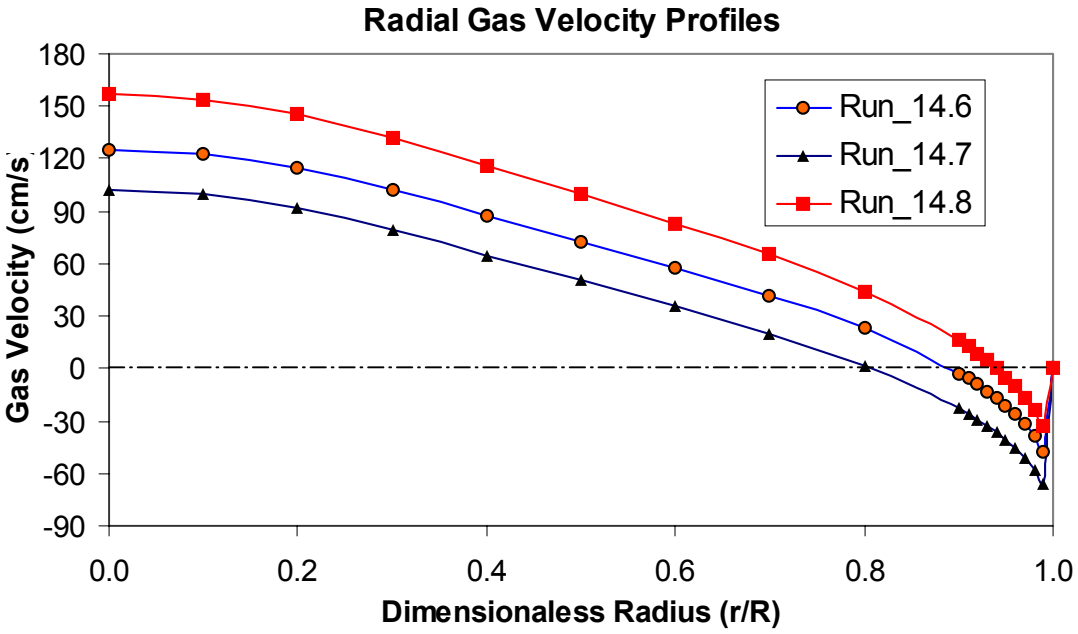

Figure 1.5 Computed 1D Gas Velocity Profiles for the Three Operating Conditions

2. NUMERICAL SIMULATION OF 2D BUBBLE COLUMN AND QUANTITATIVE COMPARISON WITH PIV MEASUREMENTS

Recently Lin et al. (1996) and Mudde et al. (1997) used PIV in their experimental studies of two-dimensional bubble columns. They provided the detailed measurements of liquid velocity and turbulence intensities for columns of different sizes and under different operating conditions. They also studied the characteristics of the macroscopic flow structures, i.e., the central meandering plume and the companion vortical regions, by measuring their frequency, wavelength and moving speed. This information yields a better understanding of the fluid dynamics in a 2D bubble column and provides a database for further numerical investigations.

Most of the previous numerical studies reported in the literature compare the predictions with the experimental measurements in a qualitative manner, while only a few quantitative comparisons are made. Therefore, although qualitative comparisons seem satisfactory in general, limited conclusions regarding the validation and reliability of numerical predictions can be drawn from these studies. This is, perhaps, partially due to the difficulties in obtaining reliable measurements in multiphase systems. It also reflects the fact that most numerical studies used the Eulerian/Lagrangian approach, which is limited to low-speed/dilute cases, while most experiments are conducted under more realistic conditions of higher gas velocity and holdup. With experimental techniques being developed and improved, it seems that the numerical study is somewhat lagging. While most experiments are limited to laboratory scale, industrial needs for reliable numerical simulations of large-scale columns are real. A computer code for such simulations should be able to deal with the situations involving large gas velocity, high gas holdup and churn turbulent flows. A key step towards this goal is to validate the numerical results, in a quantitative way, by experimental measurements. As mentioned above, the studies of Lin et al. (1996) and Mudde et al. (1997) provide reliable and extensive data on bubbly flow between two narrowly separated plates. Their experiments can be approximately simulated by solving a set of two-dimensional equations. By doing so, one should be able to utilize their measurement results, both for time-averaged and for the transient properties, to validate the numerical prediction. In addition to the mean values, the comparison of the transient properties is of particular importance since it is related to the back mixing and turbulence in the column. The testing of various physical models needed for closure can also be accomplished relatively readily in two-dimensional simulations, in comparison with the three-dimensional simulations.

In this study we present an Eulerian/Eulerian dynamic simulation of a two-dimensional bubble column. The ensemble-averaged equations are used to solve the velocity and volume fraction field for both phases. A model of bubble-induced turbulent viscosity is incorporated into the momentum equations for the liquid phase. The numerical predictions of the macroscopic structures and mean properties are compared with the experimental data provided by Mudde et al. (1997) and Lin et al. (1996). Our objective is to verify the applicability and accuracy of the Eulerian/Eulerian method for the dynamic simulation of bubble-driven two-phase flow in two-dimensional bubble columns. In this report some of the results are discussed.

2.1 Simulation Conditions

The simulations were performed for the 11.2-, 15.2- and 10.16-cm columns. The flow conditions are listed in Table 2.1. These conditions match the experiments by Lin et al. (1996) and Mudde et al. (1997). The runs for the 11- and 15-cm columns compare mean properties, while the runs for the 10-cm column provide the characteristics of large structures and their variations with superficial gas velocity.

Table 2.1 Column Size and Operation Conditions of the Cases Simulated

Column Width W (cm)	Superficial Gas Velocity U_{sup} (cm/sec)	Static Liquid Height H (cm)	Number of Gas Injectors	Aspect Ratio
11.2	1.0	110	2	9.8
15.2	1.0	110	3	7.2
10.16	1.22	160	2	15.8
	2.44	160	2	15.8
	3.66	160	2	15.8
	5.49	160	2	15.8

2.2 Governing Equations

In accordance with Drew (1983), we provide the following governing equations for the motion of gas-liquid flow in bubble columns. In these equations, the subscripts 'c' and 'd' indicate the properties for the continuous phase (liquid) and the dispersed phase (gas), respectively. The expression for the drag coefficient for the inter-phase momentum exchange is adopted from Katsumi et al. (1997) and Drew (1983). A model for the bubble-induced stress in the liquid phase, as proposed by Sato et al. (1981), is applied in the simulations.

Equations of Continuity

Liquid
$$\frac{\partial \varepsilon_c}{\partial t} + \nabla.(\varepsilon_c \mathbf{u}_c) = 0 \tag{2.1}$$

Gas
$$\frac{\partial \varepsilon_d}{\partial t} + \nabla.(\varepsilon_d \mathbf{u}_d) = 0 \tag{2.2}$$

Momentum Equations

$$\textit{Liquid}\quad \rho_c\varepsilon_c\left(\frac{\partial \mathbf{u}_c}{\partial t}+\mathbf{u}_c.\nabla\mathbf{u}_c\right)=\rho_c\varepsilon_c\mathbf{g}-\varepsilon_c\nabla p-\left(\mathbf{M}_d+\mathbf{M}_{vm}\right)+\nabla.\left(\varepsilon_c\sigma_c\right)+\nabla\cdot\left(\varepsilon_c\sigma_c^{\,b}\right) \quad (2.3)$$

$$\textit{Gas}\qquad \rho_d\varepsilon_d\left(\frac{\partial \mathbf{u}_d}{\partial t}+\mathbf{u}_d.\nabla\mathbf{u}_d\right)=\rho_d\varepsilon_d\mathbf{g}-\varepsilon_d\nabla p+\left(\mathbf{M}_d+\mathbf{M}_{vm}\right)+\nabla.\left(\varepsilon_d\sigma_d\right) \quad (2.4)$$

Inter-Phase Momentum Exchange

$$\mathbf{M}_d=\frac{6\varepsilon_c\varepsilon_d}{\pi d_p^3}\mathbf{F}_d \quad (2.5)$$

$$\mathbf{F}_d=\frac{1}{8}\rho_c\pi d_p^2 C_D\left|\mathbf{u}_c-\mathbf{u}_d\right|\left(\mathbf{u}_c-\mathbf{u}_d\right) \quad (2.6)$$

$$C_D=max\left[\frac{24}{Re}\left(1+0.15\,Re^{0.687}\right),\, f\frac{8}{3}\frac{Eo}{Eo+4}\right] \quad (2.7)$$

$$f=\left\{\frac{1+17.67\varepsilon_c^{9/7}}{18.67\varepsilon_c^{3/2}}\right\}^2 \quad (2.8)$$

where

$$Eo\equiv Eotvos\ Number\equiv g\rho_c d_p^2/\gamma$$

and $$Re\equiv Bubble\ Re ynolds\ Number\equiv \varepsilon_c d_p\left|\mathbf{u}_c-\mathbf{u}_d\right|/\nu_c$$

$$\mathbf{M}_{vm}=\frac{1}{2}\varepsilon_c\varepsilon_d C_{vm}\left(\frac{D\mathbf{u}_c}{Dt}-\frac{D\mathbf{u}_d}{Dt}\right) \quad (2.9)$$

$$C_{vm}=1+3.32\varepsilon_d+O(\varepsilon_d^2) \quad (2.10)$$

Bubble-Induced Stress

$$\sigma_c^{\,b}=\rho_c\nu_b^t(\nabla\boldsymbol{u}_c+\nabla\boldsymbol{u}_c^T);\qquad \nu_b^t=\boldsymbol{k}_b\varepsilon_d\boldsymbol{d}_p\left|\boldsymbol{u}_c-\boldsymbol{u}_d\right|;\qquad k_b=0.6 \quad (2.11)$$

2.3 Mean Properties

Figure 2.1 compares the vertical and horizontal mean velocity profiles in the 11-cm column at U_{sup}=1 cm/s. These profiles relate to the middle section of the column, where the mean flow is usually assumed to be one-dimensional. The numerical prediction of the mean horizontal velocity, $\overline{U}$, is essentially zero, as expected. However, the experimental time-averaged horizontal velocity is non-zero and exhibits an inward flow. As pointed out by Mudde et al. (1997), this is attributed to a systematic error due to the difficulty in tracking the particles in the fast-moving bubble stream and other biases. The comparison of the computed mean vertical velocity profile with data is good except for the near-wall region. One reason may be that the flow close to the walls is actually three-dimensional due to the effect of finite thickness of the columns, which is on the order of the distance to walls in the near wall region. The other reason for this discrepancy is that the boundary layer is too thin to be resolved in our current simulations. Notice that the curve of $\overline{V}$ starts and ends at the nearest points next to the walls on which the value of V is set to zero; this is due to the no-slip boundary condition imposed on the liquid phase during the simulation. The fact that $\overline{V}$ at starting and ending point reaches the maximal negative value clearly indicates that the boundary layer was not resolved. By examining the measured data points near the wall, one should realize that the experiment did not resolve the wall layer either. Unfortunately, the gas holdup profile was not reported in the experiments of Mudde et al. (1997); therefore, one cannot test to what extent the data satisfy the continuity equation. The numerical results do satisfy the mass balance.

For the 15-cm column, the comparisons of the computed and experimentally determined mean vertical liquid velocities are presented for the middle, lower and upper sections in Figure 2.2. Again the numerical values match the data in magnitude except in the wall region. The experimental profiles for the middle and upper sections are similar, while the one for the lower section is somewhat different. Mudde et al. (1997) argued that this is due to the fact that the flow is not fully developed in the lower section. On the other hand, the computed profiles for the three sections are almost identical. Thus, the numerical values for the upper and middle sections are higher in magnitude than the experimental values. The discrepancy between the predictions and data in the near wall region may be attributed to the effect of finite thickness of the third dimension. In experiments, the "two-dimensional" flow was realized between two narrowly separated plates. The distance between the plates was 1.27 cm. In the near-wall region the flow is really rather three-dimensional. Thus the slowing down of fluid by the wall in the third dimension, i.e., the parallel plates, becomes significant. However, this effect is not accounted for in the two-dimensional simulations. Since the thickness of the boundary layer is inversely proportional to the velocity, we would expect this type of discrepancy to be reduced as velocity increases. In fact the profiles for the lower section in Figure 2.2, where the velocity is high in magnitude, exhibit this trend.

The numerical predictions of turbulence intensities, $\overline{u'u'}$ and $\overline{v'v'}$, and Reynolds shear stress, $\overline{u'v'}$, for the 15-cm column operated at U_{sup}= 1 cm/s are compared with data in Figure 2.3. The $\overline{u'u'}$ reaches a peak at the central portion of the column since u attains its highest magnitude in

the center due to the nature of the meandering motion of the central plume. The peaks of $\overline{v'v'}$ at the near-wall vortical region are consistent with the fact that the flow dynamically changes from upward to downward in such areas. Although the general trends of the numerical values match the data, there are significant differences in values. It is clear that the simulation under predicts the turbulence-related properties. In reality, for the cases of low gas velocity, bubbles retain their identity, while they rise up through the column. The drag force is thus always concentrated in the liquid surrounding the bubble. However, in the Eulerian/Eulerian approach, bubbles are not identified as single identities. Although the drag force is calculated based on the single bubble formulation, it is not confined to the region adjacent to the bubbles, as it should be; rather it is more "dispersed" in the liquid. (This is obviously the inherent drawback of using the two-fluid model to describe two-phase flows at low gas holdup.)

2.4 Characteristics of Large Structures

The dynamic behavior of the large structures is characterized by the wavelength and frequency of the meandering central plume. It is expected that these quantities vary with column size and gas superficial velocity. Lin et al. (1996) have conducted an extensive and detailed experimental investigation of this topic, in 2D columns. They found that, in the same column, the frequency increases with gas velocity, while the wavelength decreases. At the same gas superficial velocity, the frequency decreases as the size of the column increases. The wavelength is proportional to the column size. When the wavelength and frequency are multiplied to give the vortex descending velocity, they found that it is basically a function of the superficial gas velocity only. They also found that the size of these vortices is independent of gas velocity when $U_{sup} \leq 1$ cm/s and varies with column size only.

To study the variation of large-scale structure, i.e., the frequency and wave length, with gas velocity we conducted a group of simulations for the 10.16 cm column. The flow conditions, as listed in Table 2.1, match the experiments done by Lin et al. (1996). Figure 2.4 shows the flow patterns when the column is operated at four different superficial gas velocities. Consistent with the experimental observation, wavelength decreases as the gas velocity increases. The overall gas holdup increases as U_{sup} increases. As the gas velocity increases, one can observe that the turbulence is intensified and the flow structure becomes less clearly defined. Figure 2.5 shows the time sequences of the liquid velocity component u at a central point for each case collected at the sampling frequency of 10 Hz. The frequency clearly increases with the superficial gas velocity. The flow becomes more chaotic as gas velocity increases, while the primary frequency still remains distinguishable.

For a quantitative comparison we performed each simulation for 200 seconds after it reached the quasi steady state and recorded all the quantities. By means of flow visualization and Fourier analysis, the averaged frequency and wave length are calculated.

Figure 2.6 shows the comparisons of the frequency and wavelength of the large structure with the experimentally measured values of Lin et al. (1996). The experimental values are understood

to have been obtained visually, as implicitly indicated in their paper. We denote the frequency and wavelength of the larger structures as f_0 and λ_0, respectively. The computed values of λ_0 and f_0 are measured by the visualizations and animations of the numerically generated liquid velocity field. The other way to estimate the characteristics of the larger structures in a column is to calculate the mean frequency and wave length, $\overline{f}$ and $\overline{\lambda}$, as follows,

$$\overline{\lambda} = \frac{\sum_i \lambda_i P_u(\lambda_i)}{\sum_i P_u(\lambda_i)} \qquad \overline{f} = \frac{\sum_i f_i S_u(f_i)}{\sum_i S_u(f_i)}$$

in which $P_u(\lambda)$ and $S_u(f)$ are the spatial and temporal Fourier spectra, respectively, for the horizontal component of the liquid velocity along the central line of the column. $\overline{\lambda}$ and $\overline{f}$ are then averaged over time and space, respectively. It can be seen that the numerical values match fairly well with the measured data, particularly for the two cases of intermediate U_{sup}. We have noticed that at low and high gas velocity, the structures are not uniform over space and time, as can be seen in Figures 2.4 and 2.5. Such non-uniformity may have induced the deviations in the calculated and measured values.

The effect of the distributor, the sensitivity analysis and the effect of mesh size will be discussed in the next monthly report.

References:

Drew, D. A., "Mathematical modeling of two-phase flow," *Ann. Rev. Fluid Mech.*, 15, 261 (1983).

Katsumi, T., A. Furumoto, L.-S. Fang and J. Zhang, "Suspension viscosity and bubble rise velocity in liquid-solid fluidized beds," *Chem. Eng. Sci*., 52, 3053 (1997).

Lin, T.-J., J. Reese, T. Hong and L.-S. Fan, "Quantitative analysis and computation of two-dimensional bubble columns," *AIChE. J*., 42, 301 (1996).

Mudde, R. F., D. J. Lee, J. Reese and L.-S. Fan, "Role of coherent structures on Reynolds stresses in a 2D bubble column," *AIChE. J.***,** 43, 913 (1997).

Sato, Y., M. Sadatomi and K. Sekoguchi, "Momentum and heat transfer in two-phase bubble flow I," *Int. J. Multiphase Flow*, 7, 167 (1981).

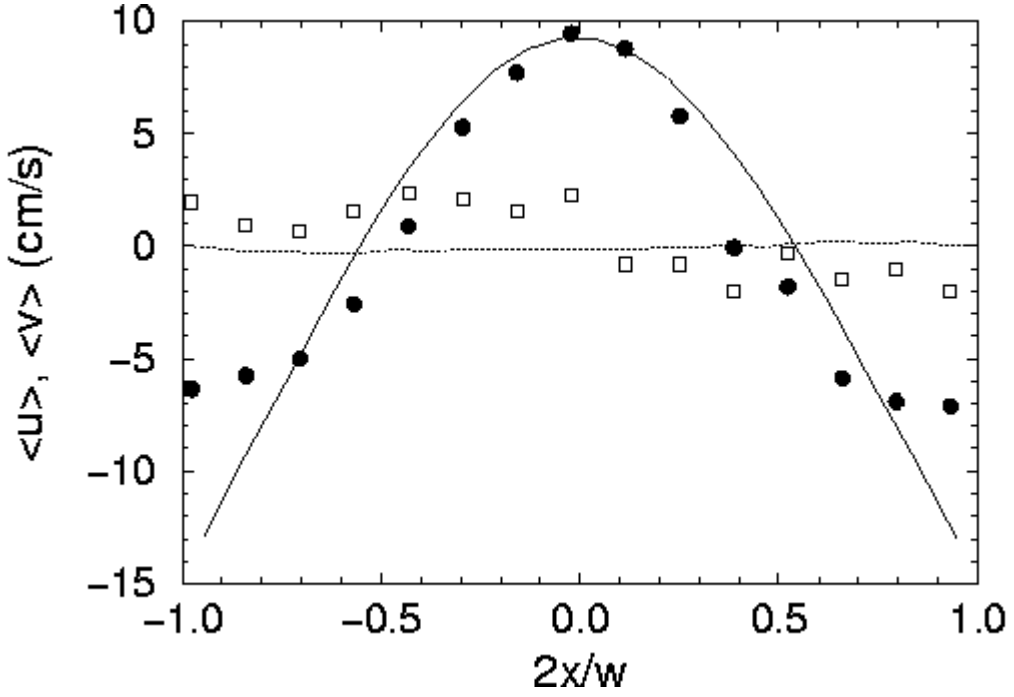

Figure 2.1 Time-Averaged Liquid Velocity Profiles for the 11-cm Column at U_{sup}= 1 cm/s. —— and --------- are the Numerical Predictions of the Vertical (Axial) Velocity Component $\overline{V}$ and the Horizontal Velocity Component $\overline{U}$, Respectively. • and Y represent the Experimental Measurements of $\overline{V}$ and $\overline{U}$, Respectively. The Experimental Data are from Mudde et al. (1997).

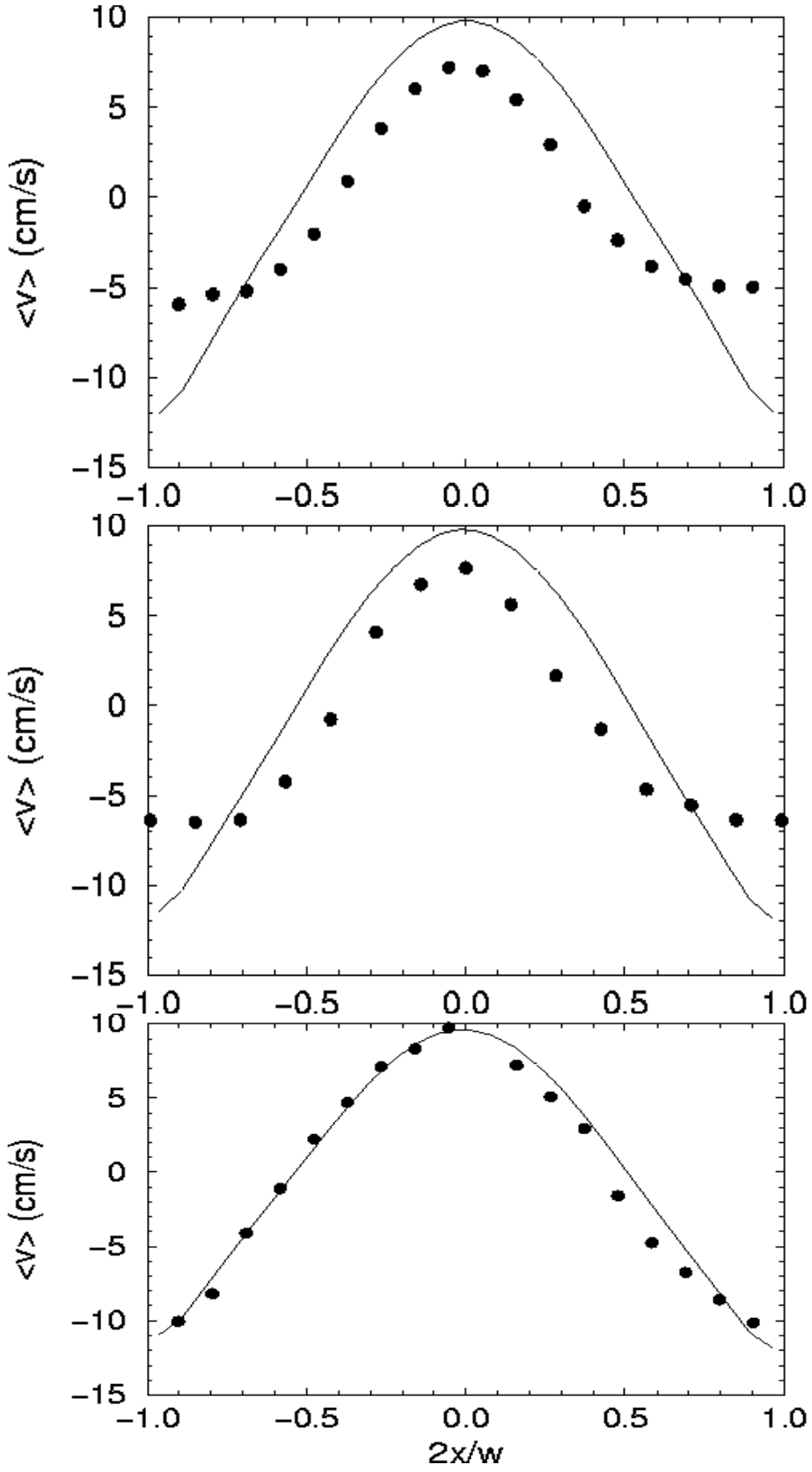

Figure 2.2 Time-Averaged Liquid Velocity Profiles, $\overline{V}$, for the 15-cm Column at U_{sup} = 1 cm/s. ——— and • represent the numerical prediction and experimental data (Mudde et al. (1997), respectively.

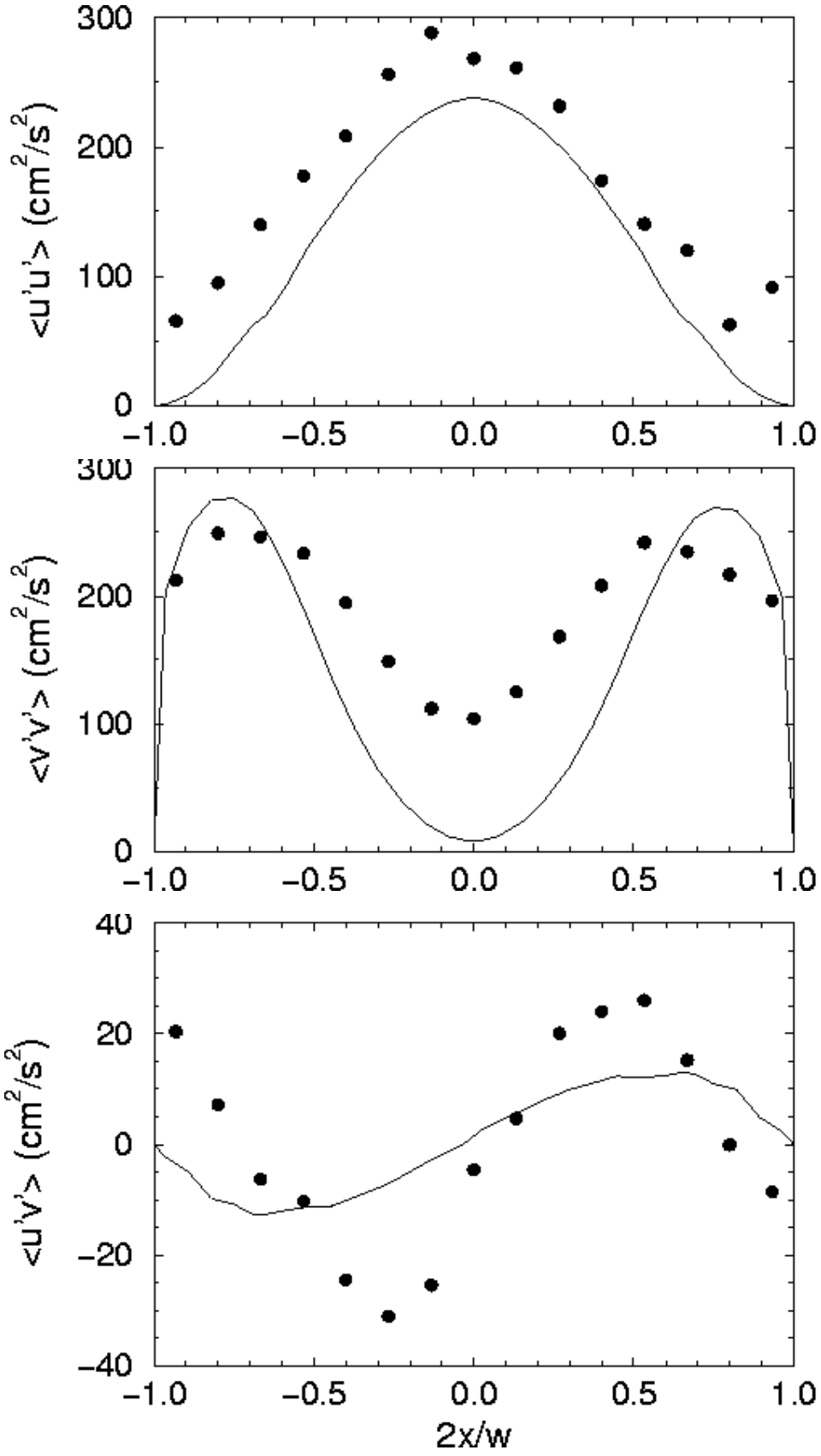

Figure 2.3 The Time-Averaged Profiles of Turbulence Intensities and Reynolds Shear Stress for the Middle Section of the 15-cm Column at U_{sup}= 1 cm/s. — and • represent the numerical values and data, respectively.

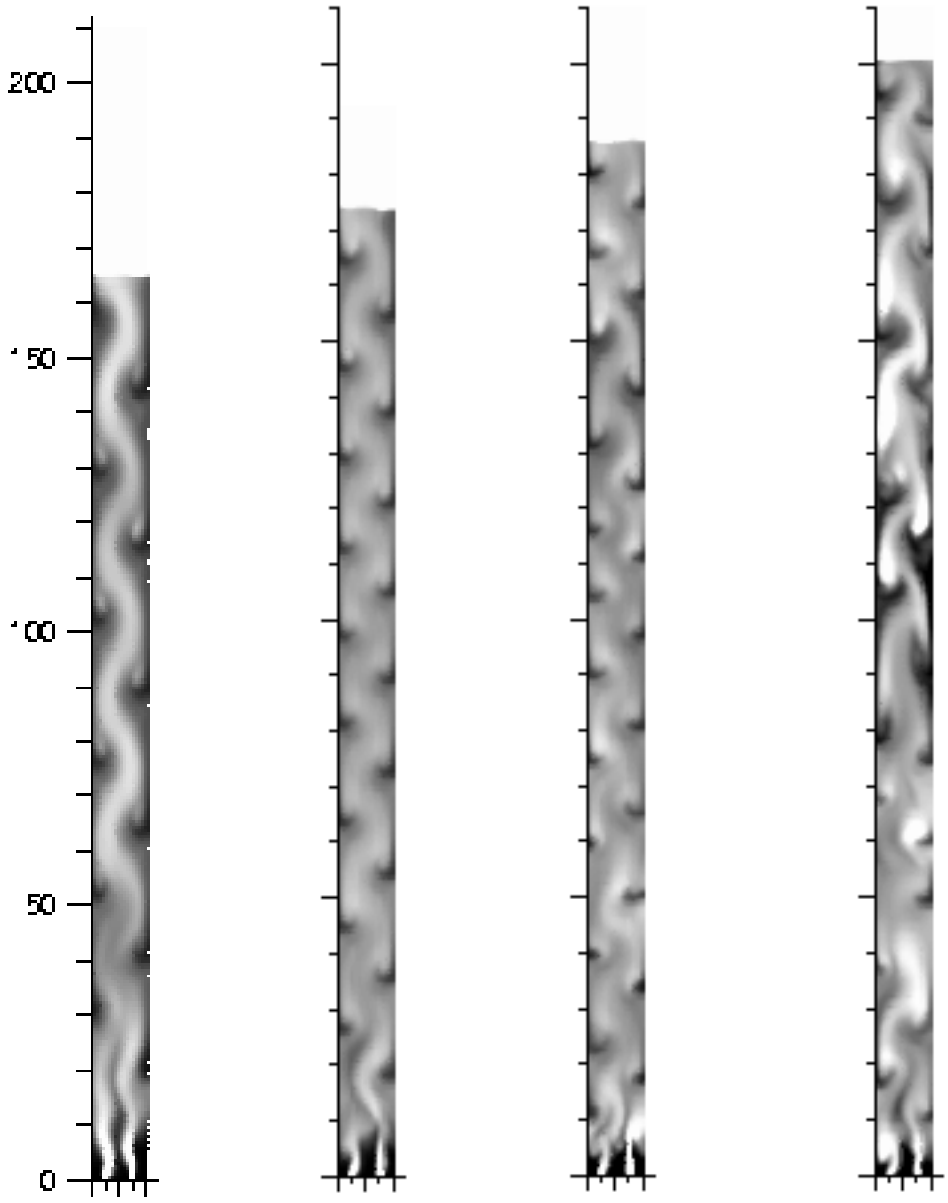

Figure 2.4 The Instantaneous Contours of Gas Holdup for the 10 cm Column Operated at Different Superficial Gas Velocity. From the left to the right, U_{sup} =1.22, 2.44, 3.66 and 5.49 cm/s.

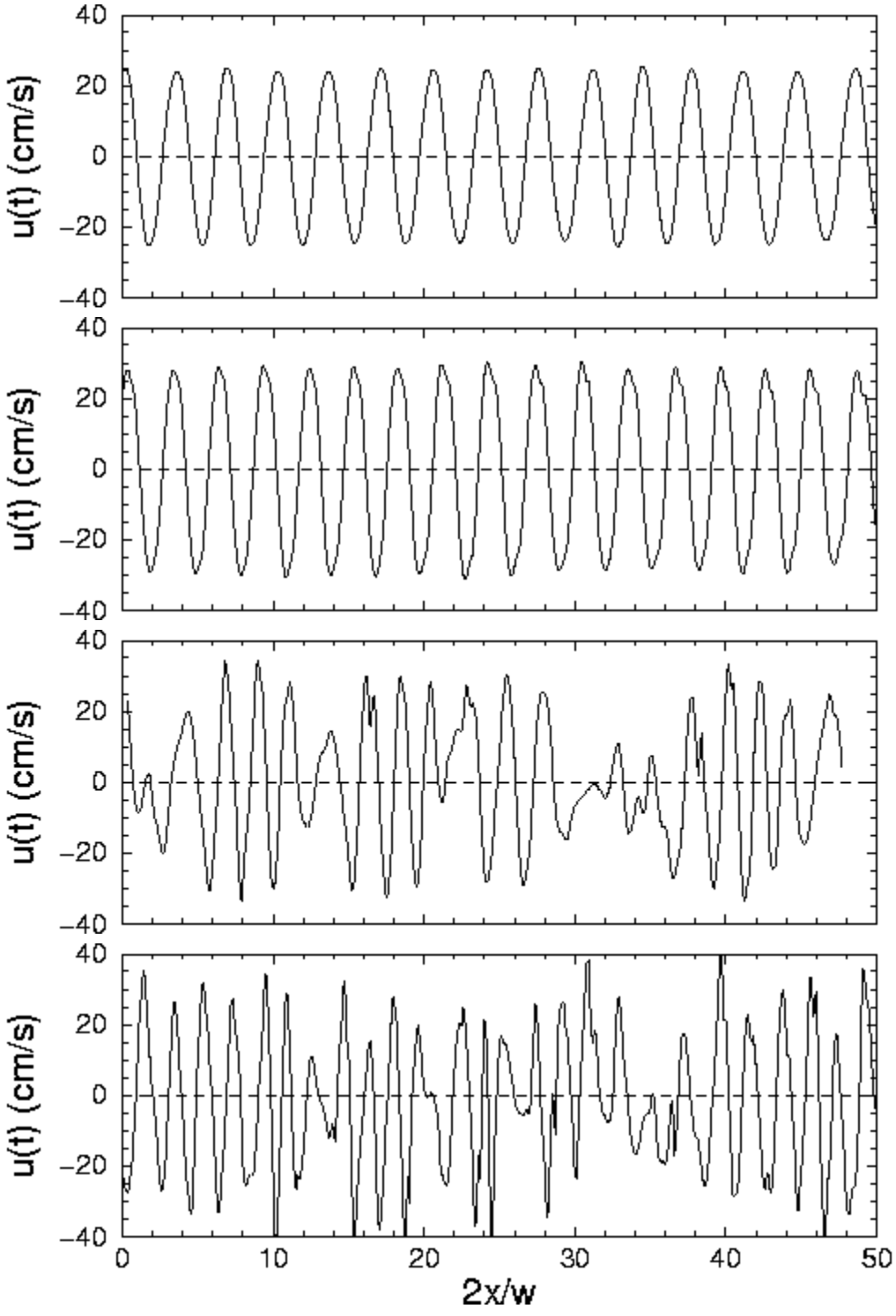

Figure 2.5 Time series of the velocity components at a central point of the 10-cm column at different $U_{sup.}$ From the top to the bottom, U_{sup}= 1.22, 2.44, 3.66 and 5.49 cm/s.

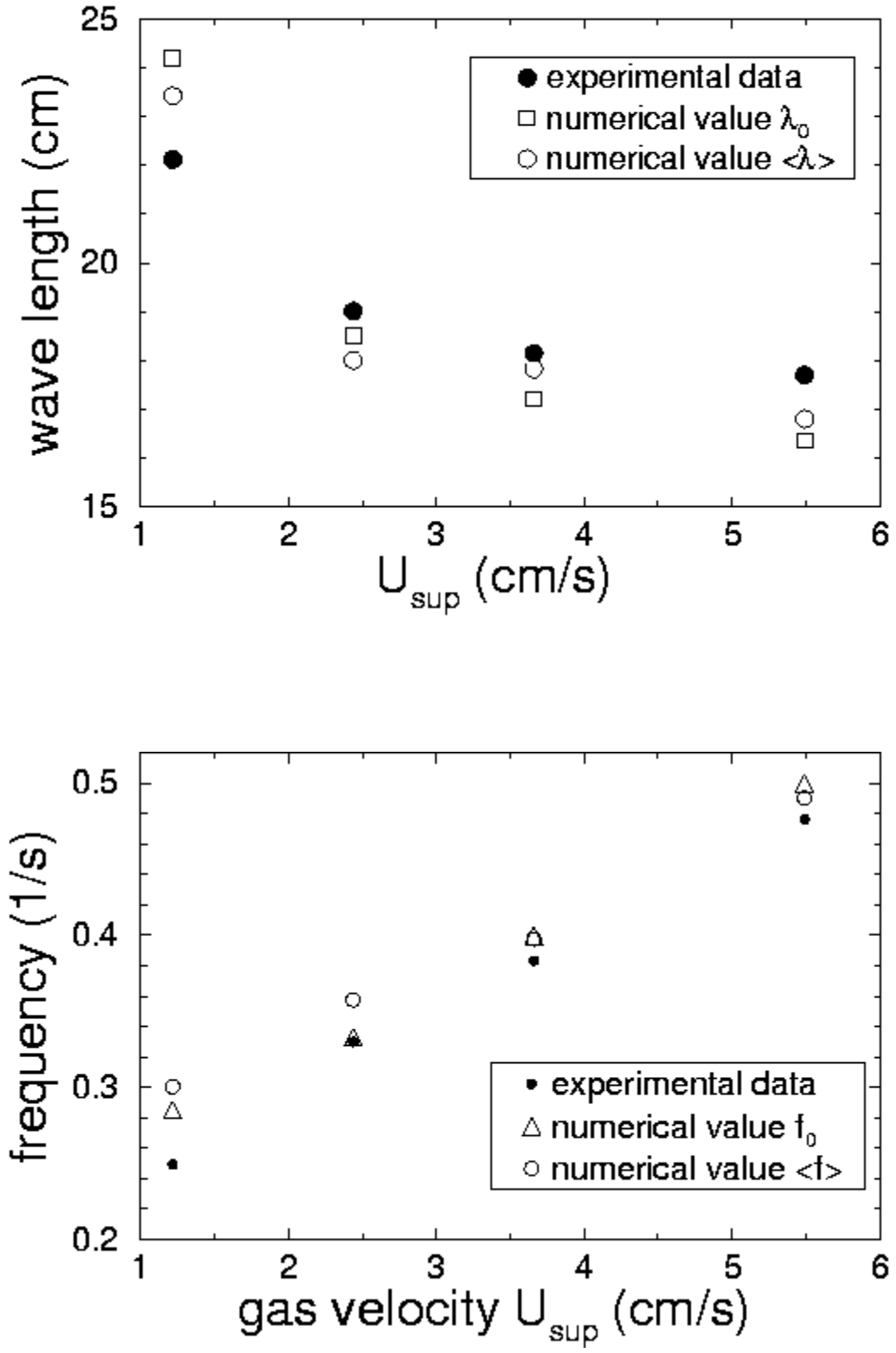

Figure 2.6 The Variation of Frequency and Wave length of the Meandering Structure in a 10-cm Column with Superficial Gas Velocity. The experimental data is taken from Lin et al.(1996).